Journal of The Electrochemical Society

Aging of Tesla's 18650 Lithium-Ion Cells: Correlating Solid-Electrolyte-Interphase Evolution with Fading in Capacity and Power

Aging of Tesla's 18650 Lithium-Ion Cells: Correlating Solid-Electrolyte-Interphase Evolution with Fading in Capacity and Power

M. Uitz,[a,z] M. Sternad,[a] S. Breuer,[a] C. Täubert,[b,*] T. Traußnig,[b] V. Hennige,[b] I. Hanzu,[a] and M. Wilkening[a]

[a]*Christian Doppler Laboratory for Lithium Batteries, Institute for Chemistry and Technology of Materials, Graz University of Technology (NAWI Graz), 8010 Graz, Austria*
[b]*AVL LIST GmbH, 8020 Graz, Austria*

The long-term performance of commercial lithium-ion batteries used in today's electric vehicles is of utmost importance for automotive requirements. Here, we use Tesla's 18650 cells manufactured by Panasonic to elucidate the origins of capacity fading and impedance increase during both calendar and cycle aging. Full cell testing is systematically carried out at three different temperatures (25°C, 40°C, 60°C). The cells are galvanostatically cycled at different C-rates (0.33 C – 1 C) and calendar aging is monitored at 4 different state-of-charges (SOC). Operation at high temperatures turns out to have the largest effect on both the capacity and direct current (DC) impedance. As an example, after 500 cycles at 25°C and 40°C capacity fading is approximately 12%, while at 60°C the fading reaches 22%. Our DC impedance measurements reveal the same trend. Post mortem analysis indicate that aging is strongly related to changes of the solid electrolyte interphase (SEI). Hence, the changes in performance are correlated with the change in composition (and thickness) of the SEI formed. In particular, we quantitatively measure the formation of electrically insulating LiF and find a correlation between overall DC impedance of the cells and lithium fluoride of the SEI.
 [DOI: 10.1149/2.0171714jes]

Manuscript submitted August 31, 2017; revised manuscript received October 9, 2017. Published November 15, 2017.

For years to come, Li-ion batteries are considered as one of the most attractive energy storage devices for electric vehicles. They benefit from a high specific energy density combined with a good cycle life. In order to further enhance conventional lithium-ion technology it is necessary to develop new materials and to improve existing battery concepts including, e.g., also the ways how cells are fabricated on an industrial scale. In particular, the latter includes aging studies on commercially available batteries. Such studies are essential for predicting the practical lifetime of the batteries and for assisting in identifying the main failure mechanisms that may, for example, involve lithium plating, passivating surface films properties, co-intercalation, dissolution or electrochemical re-plating of metal ions.

In particular, for automotive applications, where long cycle and calendar life is indispensable, accurate knowledge about the origins of battery aging is a major point of interest since it helps predict the operational lifetime of the systems. Understanding and identifying the main failure mechanisms, induced by certain operating conditions, would be a significant step forward in terms of reliability and lifetime costs of electric vehicles. Due to the fact that battery aging is a very complex matter, which is sensitively influenced by many factors such as temperature, storage and operating conditions as well as the types of active materials or electrolytes used, the variety of studies that focused on different aging phenomena is immense. Studies range from detailed material and component tests, e.g., on electrolytes, anodes and cathodes used, to investigations on fully commercial systems. As early as 1979 Peled[1,2] introduced the idea of the formation of a passivating surface layer, the well-known but still not fully understood solid electrolyte interphase (SEI). Typically, this SEI forms in reductive conditions at the negative electrode, i.e., the anode. In the 90s Aurbach and co-workers[3–6] and the Besenhard's group[7,8] studied the surface/interface chemistry between electrolyte and electrodes, e.g., metallic lithium and carbonaceous active materials. These pioneering studies lead to a better understanding of the SEI formation, which remains one of the major issues of battery aging. Vetter et al.[9] summarized the causes, effects and factors influencing the main aging mechanism in lithium-ion batteries, namely capacity fading and an increase of the overall impedance of the cells. Aurbach et al.[10] described four main reasons for capacity fading of lithium-ion batteries, which can be ascribed to the degradation of (i) the carbonaceous materials used as active species, (ii) the electrolyte solution, (iii) the active mass of the cathode and (iv) the surface reactions on both electrode surfaces. In particular, the formation of the SEI is supposed to be one of the main sources for the increased impedance of aged cells.

Important chemical SEI components of cells with graphite anodes and electrolytes, containing cyclic carbonates mixed with $LiPF_6$ as conducting salt, are mainly organic compounds such as lithium alkyl carbonates ($ROCO_2Li$)[4,5,11,12] as well as inorganic degradation products such as Li_2CO_3[4,5,11,12] and LiF.[5,12] Well-known electrolyte additives, such as vinylene carbonate, react with the anode to a further class of products.[13,14] Several factors limit the long-term performance of Li-ion cells: (i) chemical and mechanical stress because of extended deep cycling causes repeated anode dilatation, (ii) operation at elevated temperatures and (iii) undesired contaminations of the electrodes or the electrolyte, e.g., with traces of H_2O, generally result in accelerated electrochemical aging of the batteries. During long-term operation the SEI layer thickness increases and the interphase is continuously enriched with the inorganic decomposition products such as carbonates or fluorides,[15] see above. Contrary to the carbonaceous decomposition products, LiF is analytically detectable by ion-exchange chromatography in a quantitative way. This approach might establish a route to correlate the formation of LiF with the state-of-performance of the anode. In a non-negligible way, SEI formation at the anode side will contribute to the overall aging and loss of performance of a given Li cell.

As an introductory example, Figure 1 displays data acquired from an earlier but not yet published aging study. The study puts emphasis on the development of an analytical way to quantify the evolution of inorganic SEI components with increasing operation time of a full cell, i.e., with the growth and change of the passivating solid electrolyte interphase. For that purpose, cycle aged anodes of commercially available graphite/lithium iron phosphate (LFP) full cells (A123) were investigated post mortem after severe cycling. Figure 1 reveals that the formation of Li- and F-containing species, in both inorganic and organic compounds, on the anode clearly increases with cycle number. In particular, the analysis of F traces seems to be an appropriate tool to study the correlation between composition changes as well as the growth of the SEI, and, the increase in overall full cell resistance with cell aging. Here, we used this idea to systematically investigate the response of commercially available Panasonic Tesla

*Electrochemical Society Member.
[z]E-mail: marlena.uitz@tugraz.at

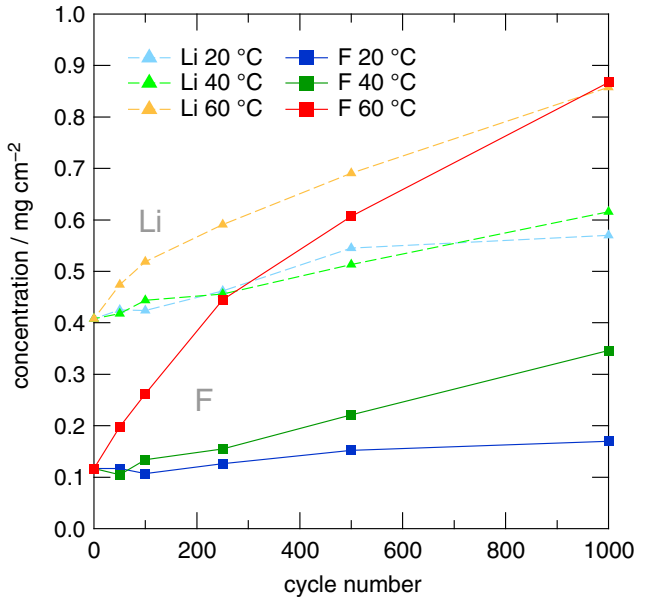

Figure 1. Change of the fluorine and lithium concentration in the anodic SEI (surface load) of commercially available A123 cells, using graphite and $LiFePO_4$ as active components, upon charging and discharging at different temperatures.

Model S batteries upon aging as a function of (i) calendar aging, (ii) cycle aging and (iii) temperature. In contrast to other aging studies, where mostly individual battery components are systematically aged, we studied full cells for a defined number of cycles. Capacity fade as well as DC impedance increase was measured after every aging step. The decision to use Tesla cells was made for the following reasons: (i) the aging behavior of cells actually used in an electric vehicle are of high potential interest and (ii) the Panasonic cell allows a disassembling of the cell components without destroying the SEI. It is sometimes difficult to separate the anode from the separator because they stick together due to SEI growth – this situation was not met in the present case. After post mortem analysis of the anode we found a strong correlation of SEI change with the formation of inorganic salts at the electrode-electrolyte interface. We attribute the clear-cut increase in full cell impedance of the 18650 cells to the evolution of the insulating SEI. The parameter chiefly influencing SEI formation is the temperature.

Experimental

Galvanostatic cycling.—The electrochemical characterization of the 18650 Tesla cells used was carried out using a MACCOR 4000 series battery cycler. Data was processed with the corresponding MIMS client v1.4 software. The cells were cycled between 4.2 V (end of charge; 100% SOC) and 2.5 V (end of discharge; 0% SOC). All electrochemical tests were carried out at three different temperatures viz. 25°C, 40°C and 60°C in air atmosphere using a forced-circulation temperature controlled chamber (Weiss Umwelttechnik, 125SB) to guarantee constant cell temperature. According to the different aging steps (see Results and discussion section), different charging and discharging rates were used ranging from 0.33 C to 1 C.

The standard capacity evaluation procedure at 25°C, which was carried at the beginning of the aging study and after every aging step, was the following: charging of the cells with 0.33 C constant current (CC) to 4.2 V (100% SOC), followed by a constant voltage (CV) step of 4.2 V until the current has decreased to C/45, which was normally reached after 1 h. After a 2 h rest period the cells were discharged with 0.5 C CC to 2.5 V (0% SOC).

For the evaluation of the DC impedance we applied a five seconds 4 C discharge pulse after an open circuit voltage (OCV) period.

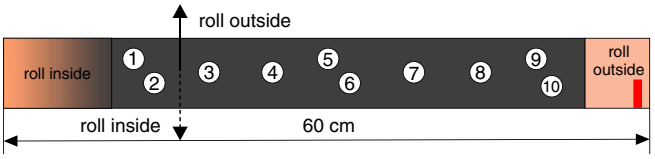

Figure 2. Location of sample spots across the anode strip of the 18650 cell used to analyze the inorganic decomposition products formed.

The following equation was used to calculate the direct current (DC) resistance R_{DC}:

$$R_{DC} = \frac{U_I - U_0}{I_0 - I_I}$$

Voltage U_0 and current I_0 were taken just prior to the pulse, whereas U_I and I_I were recorded at the end of the pulse.

Post mortem analysis.—Both cycle aged and not aged cells were analyzed post mortem. The cells were discharged to 2 V followed by a 2 V CV step for 6 h to ensure complete lithium extraction from the anode without applying abuse conditions. For our post mortem analysis the cells were dismantled in an argon-filled glove box (H_2O < 1 ppm; O_2 < 1 ppm). After disassembling the components of the jelly-roll, samples, i.e., electrode discs with a diameter of 20 mm were punched out at different locations of the unrolled graphitic anode (see Figure 2) to investigate whether uniform or non-uniform aging took place. The connection of the current collector with the negative pole (the connection tab) of the housing is located at the outside of the roll (marked in red). This means that sample 1 is at the inner side of the jellyroll at the farthest point from the negative connection tab, whereas sample 10 is at the outer side, the closest to the connection tab. The area marked with roll inside was not used due to exfoliation of the active material caused by narrow winding. Additionally, we took SEM images to investigate the different areas of the electrode.

Each sample was transferred into a separate vial and washed with DEC (diethyl carbonate) three times to remove any $LiPF_6$ as well as any residuals of the electrolyte in the pores of the anode. Afterwards we dried the samples outside the glove box in vacuum at 60°C overnight. To detach the graphite composite anode from the copper current collector and, consequently, dissolve the SEI components, we added 10 g of Millipore water (into each vial) and mixed the resulting solution. To ease and guarantee the full elution of the SEI components, e.g., LiF, we placed the containers with the samples and Millipore water in an oven (60°C) for 24 hours. Please note, the solubility of LiF in water is approximately 3 g L^{-1}, meaning that for 10 g of water we could dissolve 30 mg of LiF, which is by far more LiF than our samples contain. The whole mass of the 20 mm electrode disc, after having subtracted the copper current collector, is approximately 70 mg. The resulting aqueous solutions were quantitatively analyzed to obtain information about the Li and F concentrations, which refer to the amount of Li-containing compounds and LiF formed at the electrode surface.

The determination of fluoride concentrations was performed via anion-exchange chromatography (Dionex, USA). We used Chromeleon V6.8 SR14 (build 4522) software to quantify the amount of fluoride ions. The chromatograms were recorded with a runtime of 12 minutes. Li content was analyzed with the help of an Agilent 7500ce ICPMS (Agilent Technologies, Germany). For each sample 5 replicates were analyzed and reported as average value. For data analysis Mass Hunter 4.2 Workstation (Version C.01.02) was used. More information about aqueous sample preparation and analysis is provided in the supporting material section.

Scanning electron microscopy (SEM).—Focused ion beam cross-section cutting was employed to study the morphology and chemical composition of the SEI; in general, this method is well suited for preparing sections of porous and brittle materials. The cross-sections

were investigated with a Zeiss Ultra 55. Beside SEM pictures, which reveal the internal structure and thickness of the graphite anodes, energy dispersive X-ray spectroscopy (EDX) mapping was carried out to collect qualitative information about the distribution of fluoride-bearing components distributed over the anode surface.

Results and Discussion

Characterization of the active components of the Tesla 18650 cells.—*The anode and cathode.*—The anode consists of naturally folded graphite (see Figure 3b). As verified by EDX no other active materials, such as Si, were found in the anode. The thickness of the double-sided electrode in the initial state is approximately 98 µm on each side of the Cu current collector. The current collector itself has a thickness of 9 µm. EDX clearly shows the presence of Ni, Co and Al in the cathode pointing to the following composition of the active material $Li_xNi_{0.8}Co_{0.15}Al_{0.05}O_2$ (NCA). The cathode has a thickness of approximately 77–79 µm on each side of the Al current collector. As can be seen in Figure 3c, the cathode slurry was roll-pressed, i.e., calandered, into the Al current collector quite strongly to ensure a good electrical contact.

Electrolyte and separator.—The electrolyte of a zero aged cell was analyzed with GC-MS (gas chromatography coupled with mass spectrometry). According to our qualitative analysis the electrolyte consists of the following components: OPF_3 (phosphoroxyfluoride), which is a thermal decomposition product of $LiPF_6$;[10] DMC (dimethyl carbonate); EC (ethylene carbonate); EMC (ethyl methyl carbonate) and MPC (methyl phenyl carbonate). The exact percentage composition is unknown. In general, it was very difficult to extract some electrolyte from the jelly-roll, which was done via centrifugation. The manufacturer used only very little amounts of electrolyte. Therefore, it was only possible to qualitatively analyze the electrolyte on a non-aged cell because the electrolyte consumption within aging did not allow further sample analysis. The average pore size of the separator is 0.125 µm as verified by Hg porosimetry. The cross-section of the separator is shown in Figure 3e. The polymer part of the separator has a thickness of approximately 13 µm with an additional coating of Al_2O_3 (ca. 5 µm) on the side facing the cathode.

Electrochemical cell characterization.—As mentioned above, we used commercial high-energy 18650 lithium-ion battery cells (Panasonic) for the aging study. The typical nominal capacity of a cell is 3.03 Ah with a voltage operation window from 2.5 V to 4.2 V. The cells tested were taken from a Tesla model S electric vehicle, which was used for 6 months. After careful disassembling the cells from one of the as-received modules, the electrochemical state of the cells had to be evaluated first. For this purpose, the cells were selected on the basis of their characteristic parameters such as (i) initial capacity and (ii) DC impedance. This procedure was highly required in order to define an initial starting point (time zero) of our aging study. Then the initial capacity and DC impedance evaluation was carried

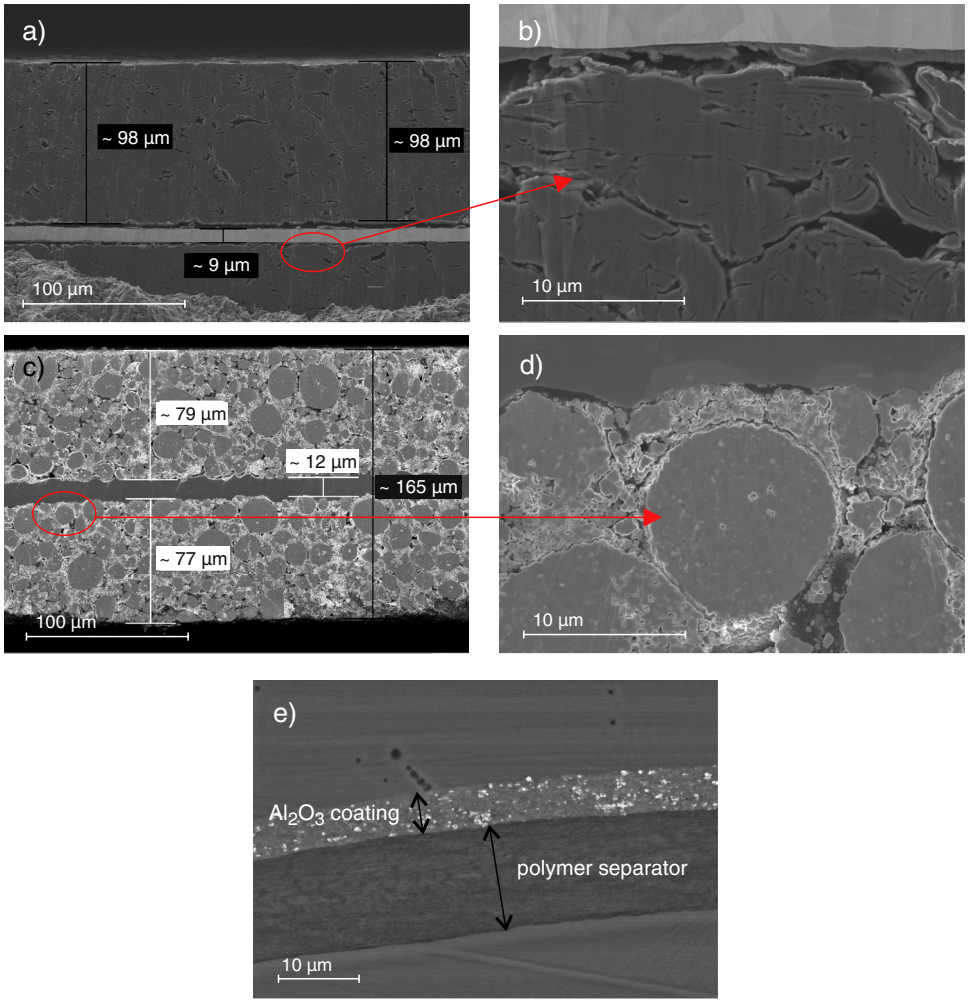

Figure 3. a) SEM images showing the focused ion beam (FIB)-prepared cross-section of the anode. The thicknesses of the current collector and the electrode are indicated. b) magnification of the naturally folded graphite seen in a). c) a FIB-prepared cross-section of the cathode; d) magnification of the NCA particles in the electrode e) cross-section of the Al_2O_3-coated polymer separator.

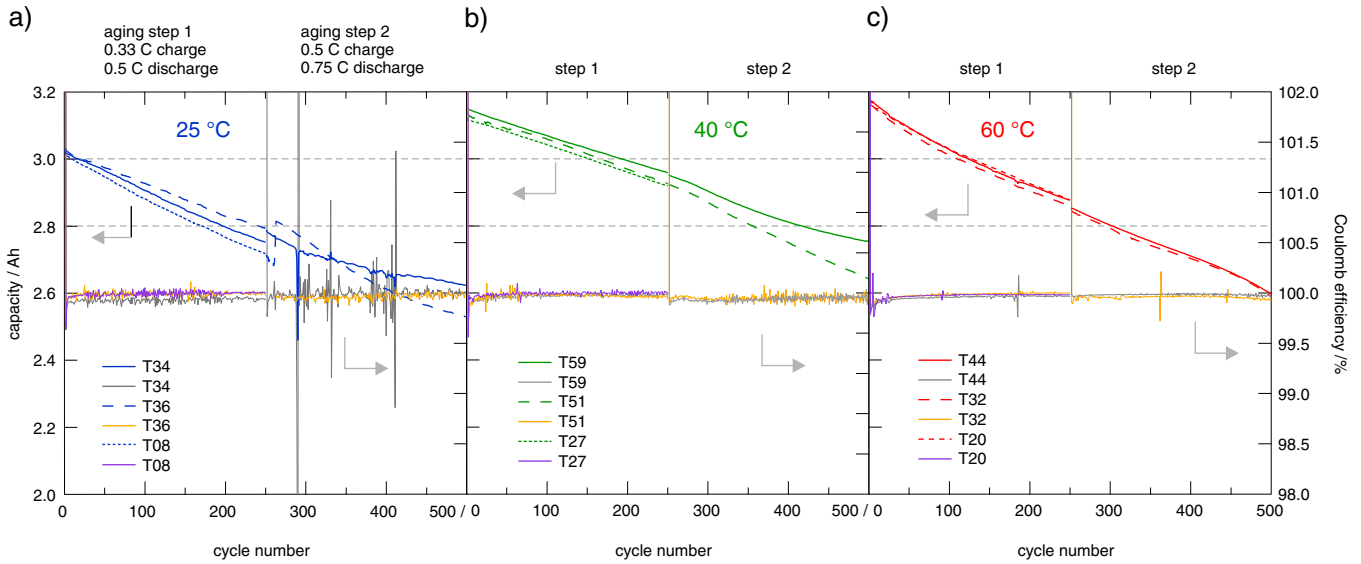

Figure 4. Discharge capacities (left axis) as determined via galvanostatic cycle aging at three different temperatures a) 25°C, b) 40°C, and c) 60°C. Aging step 1 was carried out with 3 cells per temperature with a 0.33 C charging and 0.5 C discharging rate for 250 cycles. For the second aging step, 2 cells per temperature with a 0.5 C charging and 0.75 C discharging rate for additional 250 cycles were analyzed. The vertical axis on the right refers to the Coulomb efficiencies.

out at 25°C according to the description outlined in Galvanostatic cycling section. Only cells achieving the nominal capacity and DC impedance values lower than 60 mΩ were allowed to pass through a 10 cycle galvanostatic cycling program (0.3 C CC charge to 4.2 V followed by a CV step; and 0.5 C CC discharge to 2.5 V). The cells with Coulomb efficiencies above 99.95% were selected for the subsequent cycle and calendar aging tests.

Aging of the commercially available graphite/NCA cells.—Performing reasonable aging tests requires a systematic aging test procedure. Here, all electrochemical tests were carried out at three different temperatures, i.e., at 25°C, 40°C, and 60°C with three and two cells, respectively. To ensure constant cell temperature, we placed them in a temperature chamber with forced air circulation. For cycle aging we used galvanostatic cycling to record any capacity decrease as a function of temperature. Cycle aging was separated in 2 steps with 250 cycles each; the steps only differ in the C-rates applied. After each aging step the capacity fade and increase in DC impedance was determined at 25°C according to the standard procedure described above. Calendar aging was electrochemically monitored at four different state-of-healths (SOCs), i.e., at 100%, 80%, 50%, and 20%.

For aging step 1 we cycled three cells for each temperature. The cells were charged at a CC rate of 0.33 C to 4.2 V, followed by a 4.2 V CV charging step until the resulting current decreased to C/45. The CC discharging was performed with 0.5 C until 2.5 V were reached. After completion of aging step 1 and evaluation of the capacity fade at 25°C for each cell, the cell with the highest fade per temperature was used for the subsequent post mortem analysis. The remaining 6 cells, 2 cells per temperature, were subjected to further aging according to step 2. Aging step 2 was carried out in an identical manner to step 1 except that CC rates were increased from 0.33 C to 0.5 C charging and from 0.5 C to 0.75 C discharging. Further on, in aging step 3 the CC rates were increased to 1 C for both charge and discharge step.

Calendar aging was also monitored at three different temperatures with three cells per SOC (100%, 80%, 50% and 20%). The period of aging time was identical to that of the cycle aging tests.

Cycle aging.—Figure 4 shows the cycling behavior of the first 2 aging steps at 25°C (6a), 40°C (6b) and 60°C (6c). Discharge capacities (left *y*-axis) as well as Coulombic efficiencies (right *y*-axis) are plotted as a function of cycle number.

At elevated temperatures, see data at 40°C and 60°C, we obtained higher initial capacities of approximately 3.2 Ah because of enhanced kinetics. Initial capacities at 25°C are in good agreement with the nominal capacity. The decrease of capacity upon cycling is quite similar if we consider our data recorded at 40°C (until cycle 250) and at 60°C. The capacity of each cell was measured after each aging step and related to its initial capacity to yield the capacity fade per cell. The mean values of capacity fade over the first two aging steps are summarized in Table I. It is worth mentioning that the mean values always refer to the number of cells cycled for each temperature and aging step (step 1: three individual capacity fade values are summed up and divided by three because 3 cells were cycled in the first step; in accordance to this, step 2 was calculated with 2 cells). In detail, the capacity fade is shown in the supporting material section (see Table S 3). During cycle aging it clearly turned out that temperature has a much larger effect on capacity fade as compared to the number of cycles performed. The evolution of capacity fade at 25°C and 40°C after 500 cycles shows a quite similar decrease with 12–13% of the initial value, whereas at 60°C a steeper decrease with already 22% occurs (see Table I). Obviously, the applied current, which was increased from step 1 to step 2, does not significantly influence the capacity fade measured (see Table I). Any measurable influence of the applied current would have led to a higher percental increase in capacity fade from step 1 to step 2; this is not the case here. In general, capacity fade has different origins: (i) loss of electrochemically available lithium caused by irreversible side reactions on electrode/electrolyte interfaces, (ii) loss of active material due to isolation of the particles, delamination of electrodes and contact loss, structural degradation, and (iii) increase in overall cell impedance, which reduces the available time for the battery to discharge/charge before the limiting potentials are reached.[16] Considering the Coulombic efficiencies of our study, at 40°C und 60°C the values obtained are almost constant and lie in the range of 99.95%, whereas at 25°C the dispersion is slightly higher.

Table I. Capacity fading after cycle aging (steps 1 and 2) at 25°C, 40°C, and 60°C.

Aging step/cycles	25°C	40°C	60°C
1/250	8.3%	7.6%	9.7%
2/500	12.5%	13.3%	21.9%

Table II. DC impedance growth after cycle aging (steps 1 and 2) at 25°C, 40°C, and 60°C.

Aging step/cycles	25°C	40°C	60°C
1/250	33%	53%	81%
2/500	46%	60%	138%

Additionally, the increase in DC impedance was determined after each aging step. Average values of DC impedance growth are 46% (25°C), 60% (40°C) and 138% (60°C) after 500 cycles, as shown in Table II. The increase in DC impedance is shown in the supporting material section in detail (Table S 3). Here, we observed a similar effect. The parameter mainly responsible for aging is the high temperature. These phenomena may be related to accelerated side reactions, which can occur on both electrodes, but mainly at the graphite/electrolyte interface leading to consumption and decomposition of electrolyte. As discussed already by Aurbach et al.,[10] as the surface films become thicker they cause an increase in the overall cell impedance. The main reason for this increase in impedance is expected to be caused by replacement of carbonic SEI components, e.g., Li_2CO_3, $ROCO_2Li$, with fluoridic ones such as LiF. Both LiF and Li_2CO_3 have to be regarded as poor ion conductors as their conductivities are well below 10^{-6} S cm^{-1} at room temperature (see below). However, ionic conductivity of LiF is even lower, by several orders of magnitude, than that of Li_2CO_3. As an illustration, we measured the conductivity of structurally disordered LiF, prepared by high-energy ball milling for 15 h. Although both Li cation and F anion conductivity can be enhanced by a larger concentration of structural defects, even for nanocrystalline defect-rich LiF the overall ionic conductivity does not exceed values of 10^{-13} to 10^{-14} S cm^{-1}. We took advantage of broadband impedance spectroscopy and symmetric Ag|LiF|Ag cells with ion-blocking Ag electrodes to estimate overall conductivities (see supporting material, Figure S 2). The conductivity of similarly treated Li_2CO_3 (8 h ball milling), on the other hand, turned out to be higher by some orders of magnitude; it is in the range of 1×10^{-9} S cm^{-1} (see Figure S 1 and[17]). Thus, the formation of poorly conducting LiF during aging of our cells seems to be directly correlated to the changes in electrochemical performance. To study the relationship between overall changes in cell performance and the thickness and change in composition of the SEI formed, we carried out post mortem analyses. They helped shed light on the correlation between growth in DC impedance observed and LiF formation in the SEI.

Figure 5 shows the complete cycle aging procedure including the last aging step with high C-rates. The cells exposed to 60°C and especially those treated at 40°C show failures during aging step 3 because of the high-current charging and discharging at 1 C. The exact reason for failure is unknown. It might be ascribed to the fact that the cells are designed for applications needing high-energy densities. For this reason the cells are equipped with relatively thick electrodes; most likely, they are not able to handle such high currents. The breakdown of the cells could already be predicted by the noticeable decrease in Coulombic efficiency beginning immediately after cycle no. 500. Only the cell charged and discharged at 25°C was able to withstand these operating conditions.

Calendar aging.—Table III summarizes the results of the capacity fade upon calendar aging, which was carried out at different temperatures and SOCs. It turned out that the temperature, in contrast to the situation during cycle aging, is not the only aging cause. The capacity fade observed increased in a non-negligible way with increasing SOC, reaching its highest value at 80%. Taking into account that capacity fade is always the sum of both calendar and cycle aging we end up with the result that approximately 20% at 25°C, 40% at 40°C and ca. 30% at 60°C of the total capacity fade during cycling is simply caused by calendar aging. The lowest capacity fade occurred at 20% SOC.

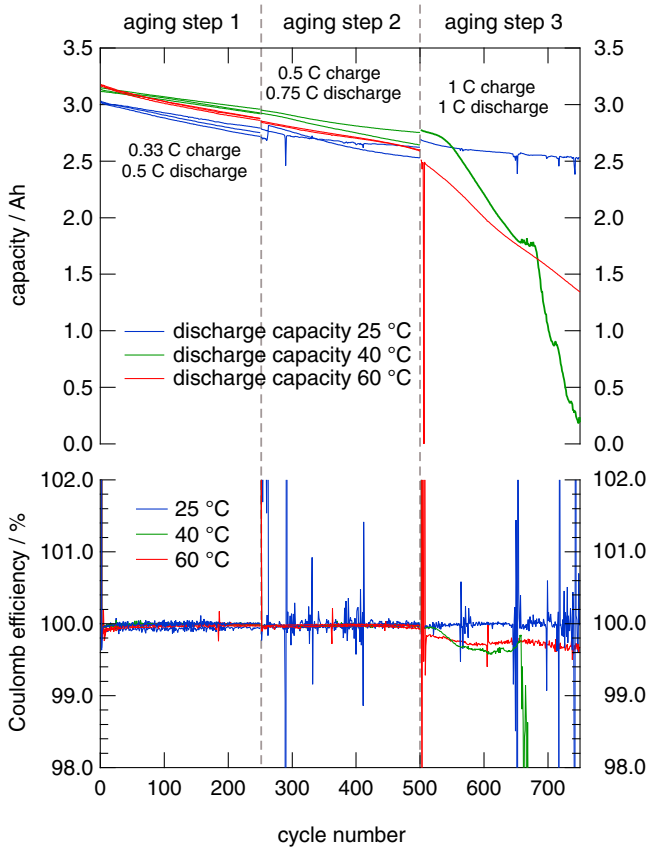

Figure 5. Aging tests performed over 750 cycles at 25°C, 40°C, and 60°C. The C-rates used are indicated. Upper panel: Capacity vs. cycle no.; lower panel: change of Coulomb efficiency as a function of cycle number.

Post mortem analysis.—To gain more information about the source of capacity fade and the increase in DC impedance, we analyzed the cells post mortem. 6 cells aged under different conditions were chosen for the analysis; another one, which was not exposed to aging, served as reference. As already described in chapter 2.4 we assume that aging, among other effects, is linked to the growth of the SEI, which is accompanied by an enrichment of LiF. Fortunately, an increasing quantity of fluoride ions can only be originated from the decomposition of the conducting salt $LiPF_6$. Through washing of the electrode samples with DEC we got rid of any electrolyte and $LiPF_6$ residuals. The elution of the dried electrode disc in water is accompanied by the elution of LiF originating from the SEI. The solubility of LiF in water is 3 g L^{-1}. Polyvinylidenfluorode-binder (PVdF), which is the only other fluoride source in the electrodes, is not soluble in water. It is, therefore, possible to study the F content in the SEI layer quantitatively via ion-exchange chromatography as a function of cycle number and temperature (see Figure 6). In Figure 6 also the Li contents are shown. We anticipate that the effect of the exact surface

Table III. Capacity fade after calendar aging (step 2 (500 cycles), depending on temperature and SOC during storage). Values are given as average ones and were calculated from three cells per SOC. The values in the brackets refer to capacity fade after calendar aging step 1 (250 cycles).

SOC	25°C	40°C	60°C
100	*(1.8)* 2.3%	*(3.5)* 3.7%	*(4.0)* 5.5%
80	*(2.2)* 2.8%	*(3.9)* 5.0%	*(5.0)* 6.6%
50	*(0.4)* 0.9%	*(1.5)* 2.7%	*(2.7)* 4.2%
20	*n.a.*	*(0.0)* 0.8%	*(1.2)* 2.3%

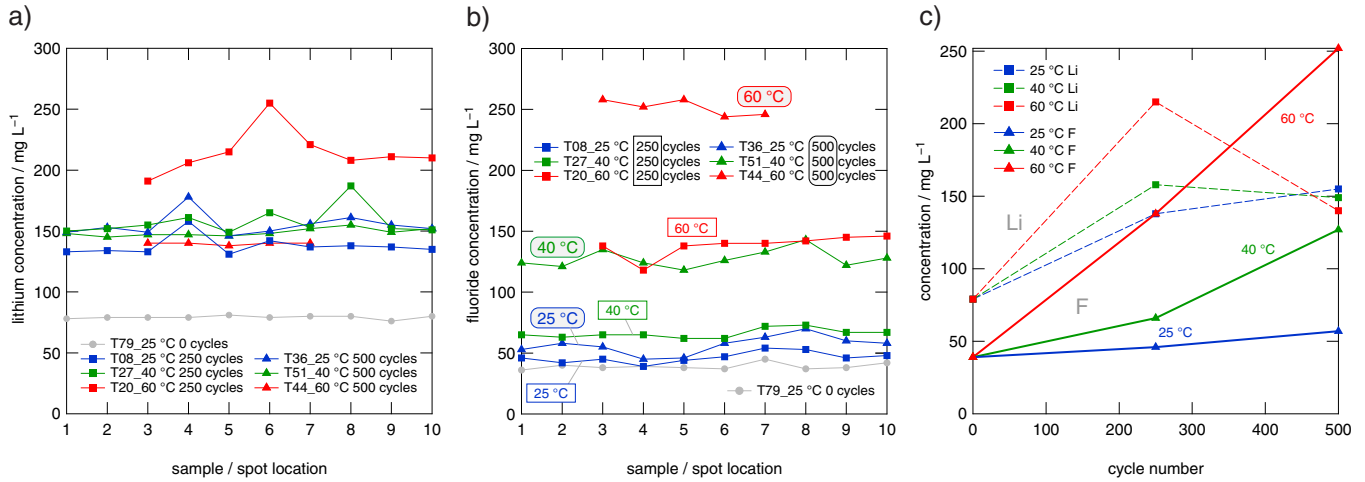

Figure 6. Quantitative evaluation of the a) lithium and b) fluoride concentration of a range of disc specimen displayed as a function of sample position, cycle number and temperature. The sample numbers represent different positions on the anode from where the specimens were punched out. Sample numbers with no data-point show cases where it was not possible to take a specimen due to exfoliation of the active material from the current collector. c) Linear change in fluoride concentration with temperature and cycle number; the change in Li concentration shows no clear correlation.

area S for each sample, which is difficult to access experimentally due to the porosity of the electrode, is negligible here. This view is supported by the fact that the Li and F concentrations seen are much larger than variations induced by different surface area values. Hence, Li and F concentrations are given in mg L^{-1} to highlight the relative change in concentration from non-aged to aged cells.

Each sample number refers to a certain position on the anode (see Figure 2), starting with 1, which is at the inner end of the jellyroll, and ending with 10, which corresponds to the disc punched out at the outer end. With this method it is possible to get some 'space-resolved', albeit only coarsely, information about the composition of the SEI. Here, we observe that the distribution of the decomposition products seems to be quite uniform over the electrode area investigated, see Figure 6.

For the Li concentrations (see Figure 6a) we obtained values of approximately 150 mg L^{-1} over the whole electrode surface; these values do not depend on temperature and cycle number. Cell T20 (250 cycles at 60°C) is the only exception with a concentration higher by 50 mg L^{-1}. Most likely, this cell was not fully discharged due to loss of electronic contact of the active material with the current collector, which leads to incomplete extraction of lithium ions from the active material during discharging. Another reason could be an insufficient washing procedure. The Li concentration of the non-aged cell is about half the value of the aged cells with approximately 79 mg L^{-1} clearly indicating that at the beginning of the battery life the surface films are thinner with less Li-bearing components.

Analyzing the F content of the SEI leads to the full picture of what took place at the electrolyte-electrode interface. Figure 6b illustrates that the fluoride concentration increases with increasing cycle number and temperature. At state of aging zero, we start with a fluoride concentration of approximately 39 mg L^{-1}. This value increases slightly after the cells were charged and discharged for 250 and 500 cycles at 25°C and 40°C, respectively. Further cycling at 40°C and 60°C causes a significant increase in fluoride concentration reaching values ranging from 127 (500 cycles, 40°C) to 138 mg L^{-1} (250 cycles, 60°C). Further charging and discharging at 60°C reaching 500 cycles results in a fluoride concentration of 252 mg L^{-1}. The data unequivocally show that temperature has an immense effect on the decomposition of the electrolyte and the enrichment of the SEI with F-containing compound. Table IV shows the fluoride concentration depending on cycle number and temperature; values are given in relative percentage with respect to the reference cell (100%). For more information on lithium and fluoride concentrations we refer to the supporting material section (Table S 1 and S 2).

Table IV. Relative fluoride concentrations as obtained from post mortem analysis. The data points represent the mean fluoride concentrations over the whole electrode area investigated.

Aging step/cycles	25°C	40°C	60°C
0	100%	100%	100%
1/250	119%	169%	355%
2/500	145%	327%	645%

To sum up, the quantitative SEI investigations revealed that at the beginning of the aging processes the amount of Li-containing SEI components increases and reaches a certain level (see also Figures 6a–6c). During further operation, the amount of lithium components hardly changes; upon further cycling, however, F-containing products are increasingly deposited at the interface. To better illustrate the change in composition, we calculated the molar concentration of Li and F, for the reference (T79) and the aged cell (T44) after the cells were exposed to 500 cycles at 60°C (see Table V). For the reference cell approximately 18% of Li is bound to F, whereas for the aged cell already 65% of Li exists in the form of LiF.

To support the results extracted from ion-exchange chromatography and to reveal the internal structure and thickness of the natural graphite anodes, before and after aging, we recorded cross-section scanning electron micrographs. In addition, we used elemental mapping to obtain qualitative information about the fluoride concentration and distribution over the graphite surface/interface. Figure 7 shows the corresponding cross-sections and EDX fluorine mapping at three different aging states. The finely dispersed F signal presumably originates from fluoride from the binder. However, as can be seen in Figures 7b and 7c an increase in fluoride signal is noticeable, supporting the quantitative analysis given above. With the help of the SEM cross-section images it was also possible to estimate the increase in electrode thickness; in the present case an increase of

Table V. Molar concentrations of Li and F depending on the aging state of the commercial cells.

LiF (1:1)	Li (mol L^{-1})	F (mol L^{-1})
0 cycles	1.14×10^{-2}	2.05×10^{-3}
500 cycles 60°C	2.02×10^{-2}	1.33×10^{-2}

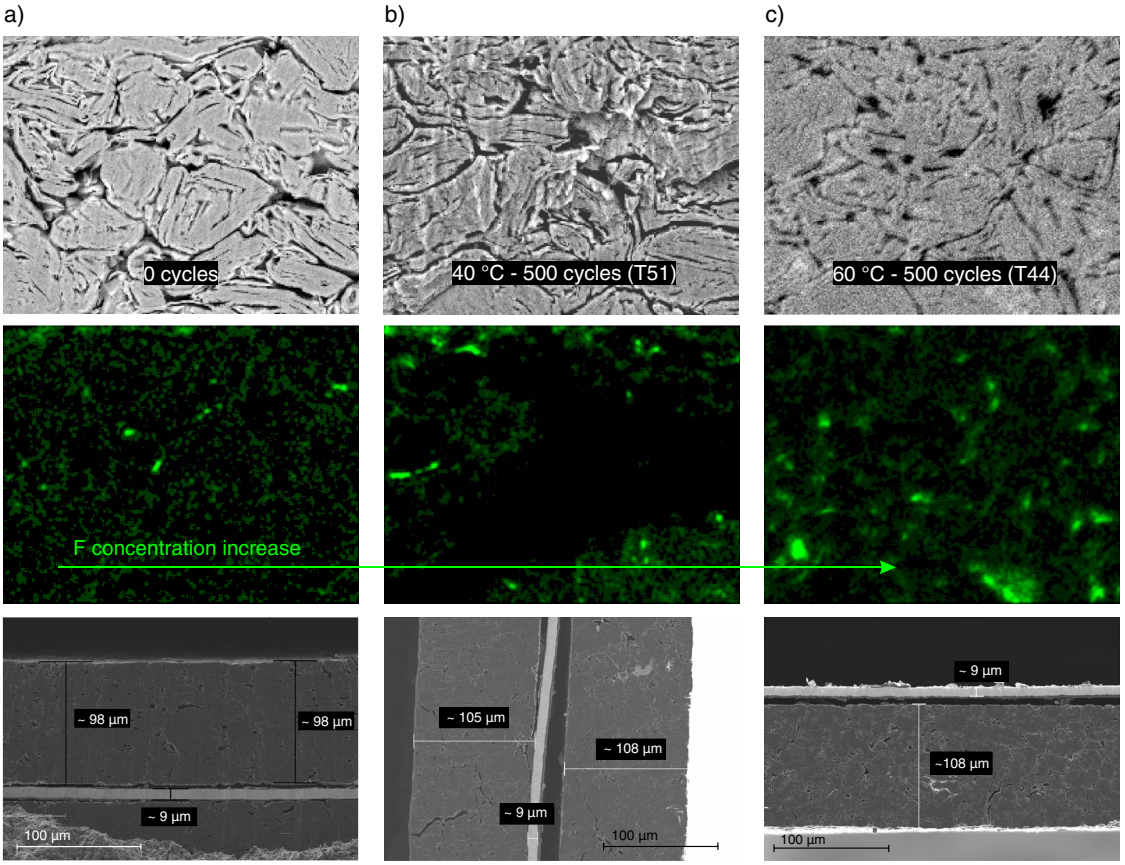

Figure 7. SEM cross section pictures (upper and lower panel) of the graphite electrodes with the corresponding results obtained via EDX fluorine mapping (middle panel); in a) sample T79 served as reference, in b) cell T51 (500 cycles, 40°C) is shown and in c) sample T44 (500 cycles, 60°C) is represented.

about 10% for cells exposed to 500 cycles at 40°C and 60°C was found.

Figure 8 combines the results obtained through electrochemical tests and post mortem analysis. We clearly witness a correlation between fluoride concentration (see Table IV) and the increase in overall DC impedance with cycle number. Figure 8b illustrates that at 60°C the increase in F concentration is directly linked with the impedance response observed. Hence, the source of impedance growth can be mostly ascribed to the enrichment of F in the SEI. The correlating behavior shows that in the present case DC impedance measurements represent a suitable tool to measure the SoH of a given cell by non-destructive means.

Beside the increase in cell impedance, capacity fade is the second important aspect related to battery aging. Bringing capacity fade

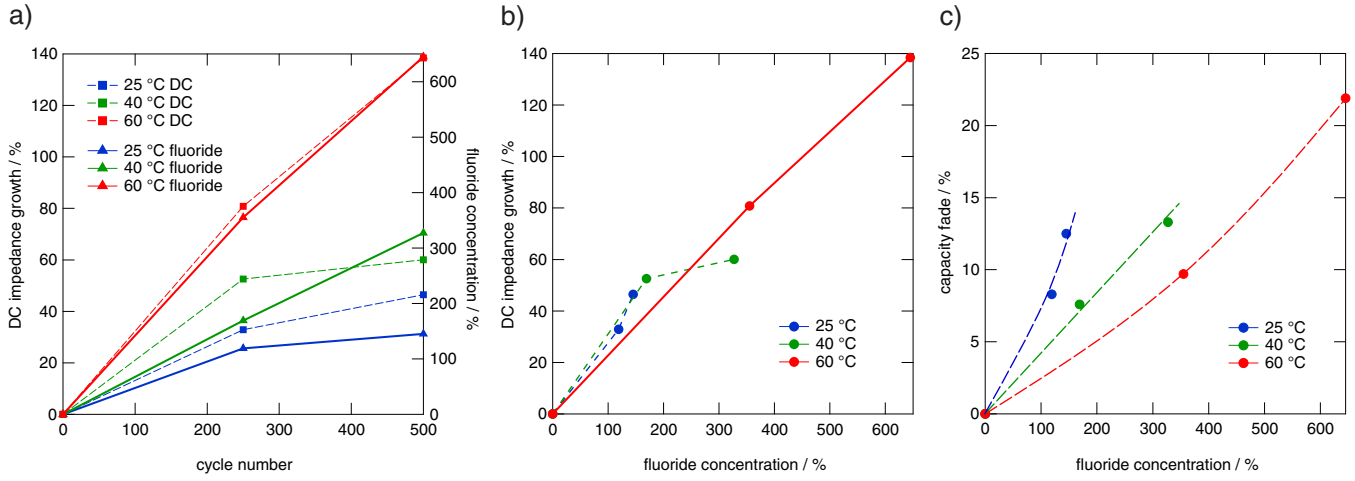

Figure 8. a) temperature-dependent relationship between DC impedance growth in %, as determined by electrochemical tests, and fluoride concentration in %, as obtained from quantitative post mortem analysis, as a function of cycle number. b) linear correlation of (i) the growth in DC impedance and (ii) fluoride concentration. The increase in DC impedance is mainly induced by the increase in fluoride concentration. c) capacity fade vs. fluoride concentration. Capacity fade is only partially caused by the increase in fluoride concentration.

and fluoride concentration into relation with each other indicates that capacity fade is only partially caused by an increase in fluoride concentration (see Figure 8c). This capacity fade can be explained as an aftereffect of DC impedance increase because of the fact that less time for charging or discharging is available caused by a higher IR drop. Hence, considering Cycle aging section it seems reasonable to assume that capacity fade is additionally influenced by other factors such as loss of cyclable lithium or active material. To look at these origins in more detail we investigated electrodes of the aged anodes separately in three-electrode half-cells. We cycled the cells vs. metallic Li, using a Li reference electrode, and recorded the available capacity. The specific capacities measured are in the order of 350 mAh g^{-1}; see supporting material section (Figure S 3). This value indicated that the whole active material is still participating in the charge/discharge processes. Thus, here the loss of electrochemically available lithium in the full cells is assumed to be mainly responsible for the capacity fade observed, see[18] for similar observations.[17]

Conclusions

In this study commercial 18650 lithium-ion battery cells were used to analyze cycle and calendar aging. Parameters such as capacity fade with cycle and calendar aging, as well as the DC impedance increase, were recorded as a function of different temperatures, storage and cycling conditions. It turned out that (i) capacity fade and (ii) the increase in DC impedance during cycle aging are predominantly driven by high temperatures rather than by the number of cycles. After 500 cycles at 25°C and 40°C, capacity fade is about 13%, whereas at 60°C the fade already reached 22%. The same trend is shown by the 46% (25°C), 60% (40°C) and 138% (60°C) increase in DC impedance observed after 500 cycles. During calendar aging capacity fade increases with increasing temperature and SOC, reaching its highest values at 80% SOC.

Correlating electrochemical performance tests with quantitative post mortem analysis on the graphitic composite anode shows that the aging effect can be linked to a change in composition of the SEI formed. Worth noting, we did not take into account effects taking place on the cathode side such as degradation of NCA. Independent of that we found that the change of the SEI at the anode side directly correlates with the change in impedance of the full cells. The change in SEI at the anode is reflected in an increase of the amount of SEI formed, i.e., its thickness, and is accompanied by an enrichment with LiF, which finally leads to the aforementioned clear increase of the impedance of the full cell. Quantitative analysis of lithium shows that, at the beginning of the aging processes, the amount of Li-containing SEI components increases up to a certain point. Further charging and discharging causes the amount of lithium to change only little. In contrast to that observation the SEI enriches in F species. Both the number of cycles and temperature controls this enrichment in LiF. Considering the whole electrode area analyzed it turned out that aging takes place in a fairly uniform way.

The observed linear correlation of fluoride concentration and growth in DC impedance leads to the assumption that the cell impedance is mainly controlled by the formation of poorly conducting LiF that progressively turns the SEI into an ionically insulating interphase. Capacity fade, on the other hand, can only partly be ascribed to the formation of LiF. The loss of mobile lithium (or electrical isolation of active material) seems to play a non-negligible role in the present case.

Acknowledgment

We thank V. Pregartner for her help with the conductivity measurements. Financial support by the Austrian Federal Ministry of Science, Research and Economy, and the Austrian National Foundation for Research, Technology and Development (CD-Laboratory of Lithium Batteries: Aging Effects, Technology and New Materials) is greatly appreciated.

ORCID

M. Sternad https://orcid.org/0000-0001-9307-222X
I. Hanzu https://orcid.org/0000-0002-9260-9117

References

1. E. Peled, *J. Electrochem. Soc.*, **126**, 2047 (1979).
2. E. Peled, *J. Power Sources*, **9**, 253 (1983).
3. D. Aurbach, B. Markovsky, A. Shechter, Y. Ein-Eli, and H. Cohen, *J. Electrochem. Soc.*, **143**, 3809 (1996).
4. D. Aurbach, B. Markovsky, I. Weissman, E. Levi, and Y. Ein-Eli, *Electrochim. Acta*, **45**, 67 (1999).
5. D. Aurbach, M. Moshkovich, Y. Cohen, and A. Schechter, *Langmuir*, **15**, 2947 (1999).
6. D. Aurbach, E. Zinigrad, Y. Cohen, and H. Teller, *Solid State Ion.*, **148**, 405 (2002).
7. J. O. Besenhard, M. Winter, J. Yang, and W. Biberacher, *J. Power Sources*, **54**, 228 (1995).
8. M. R. Wagner, P. R. Raimann, A. Trifonova, K. C. Moeller, J. O. Besenhard, and M. Winter, *Electrochem. Solid-State Lett.*, **7**, A201 (2004).
9. J. Vetter, P. Novák, M. R. Wagner, C. Veit, K. C. Möller, J. O. Besenhard, M. Winter, M. Wohlfahrt-Mehrens, C. Vogler, and A. Hammouche, *J. Power Sources*, **147**, 269 (2005).
10. D. Aurbach, B. Markovsky, A. Rodkin, M. Cojocaru, E. Levi, and H. J. Kim, *Electrochim. Acta*, **47**, 1899 (2002).
11. K. Xu, G. V. Zhuang, J. L. Allen, U. Lee, S. S. Zhang, P. N. Ross, and T. R. Jow, *J. Phys. Chem. B*, **110**, 7708 (2006).
12. S. Leroy, H. Martinez, R. Dedryvère, D. Lemordant, and D. Gonbeau, *Appl. Surf. Sci.*, **253**, 4895 (2007).
13. H. Ota, Y. Sakata, A. Inoue, and S. Yamaguchi, *J. Electrochem. Soc.*, **151**, A1659 (2004).
14. H. Ota, Y. Sakata, Y. Otake, K. Shima, M. Ue, and J. -i. Yamaki, *J. Electrochem. Soc.*, **151**, A1778 (2004).
15. C. L. Campion, W. Li, and B. L. Lucht, *J. Electrochem. Soc.*, **152**, A2327 (2005).
16. A. Barré, B. Deguilhem, S. Grolleau, M. Gérard, F. Suard, and D. Riu, *J. Power Sources*, **241**, 680 (2013).
17. D. Prutsch, S. Breuer, M. Uitz, B. Stanje, J. Langer, P. Bottke, S. Lunghammer, P. Posch, V. Pregartner, M. Philipp, A. Dunst, D. Wohlmuth, H. Brandstätter, W. Schmidt, V. Epp, A. Chadwick, I. Hanzu, and M. Wilkening, *Z. Phys. Chem.*, **231**, 1361 (2017).
18. M. Safari and C. Delacourt, *J. Electrochem. Soc.*, **158**, A1123 (2011).